Supplementary information

Size dependent structural, energetic and spectroscopic properties of MoS_3 polymorphs

Amit Sahu[1,2] , Stephan N. Steinmann[2] and Pascal Raybaud[1,2]*

[1]IFP Energies Nouvelles, Rond-point de l'échangeur de Solaize, BP3 - Solaize 69360, France

[2]Univ. Lyon, ENS de Lyon, CNRS UMR 5182, Université Claude Bernard Lyon 1, Laboratoire de Chimie, F-69342 Lyon, France

SI.1 STRUCTURAL ANALYSIS

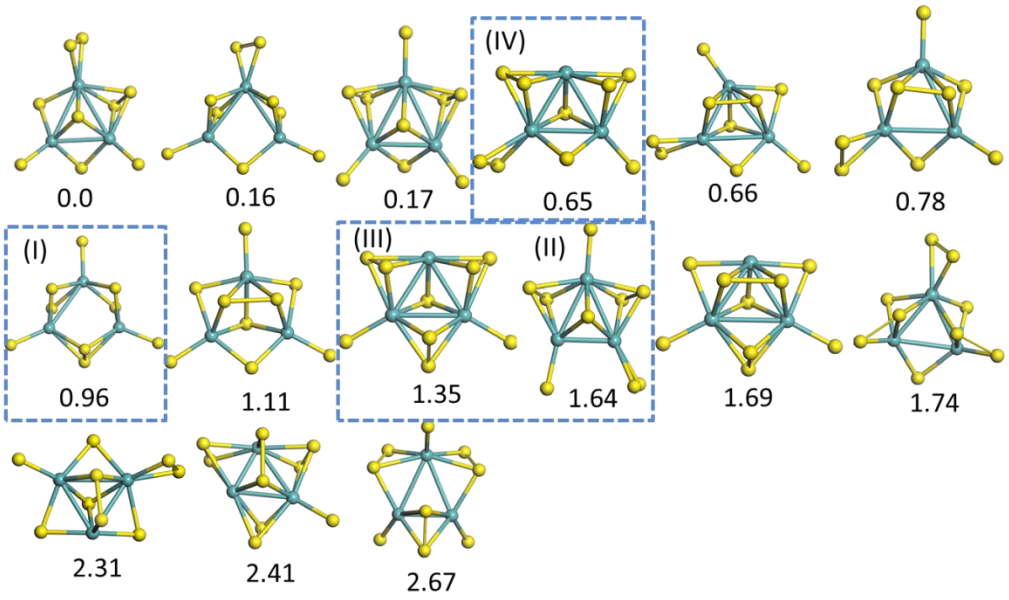

Figure S1: Various explored 0D-Mo_3S_9 clusters and their relative energy (in eV) w.r.t most stable conformer. The earlier structures (formal oxidation states of Mo is +4) proposed by Weber et al. and simulated by Jiao et al. are represented in the dashed squared frames with the original label by Weber et al. [1] To avoid the spurious interaction with its periodic images, we use a large cell 20 x 20 x 20.

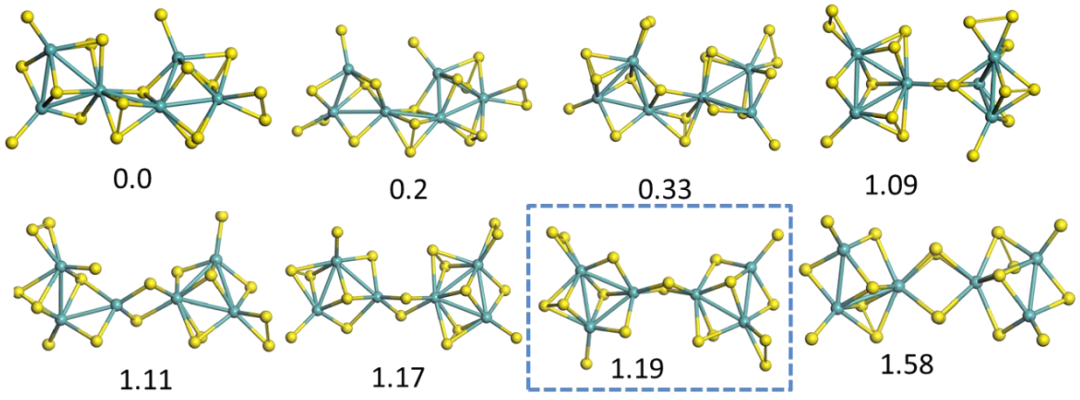

Figure S2: Various explored 0D-Mo_6S_{18} clusters (triangular dimers) and their relative energy (in eV) w.r.t the most stable one (the first one at 0.0 eV). The conformer used for the initial configuration of AIMD is highlighted by a squared frame.

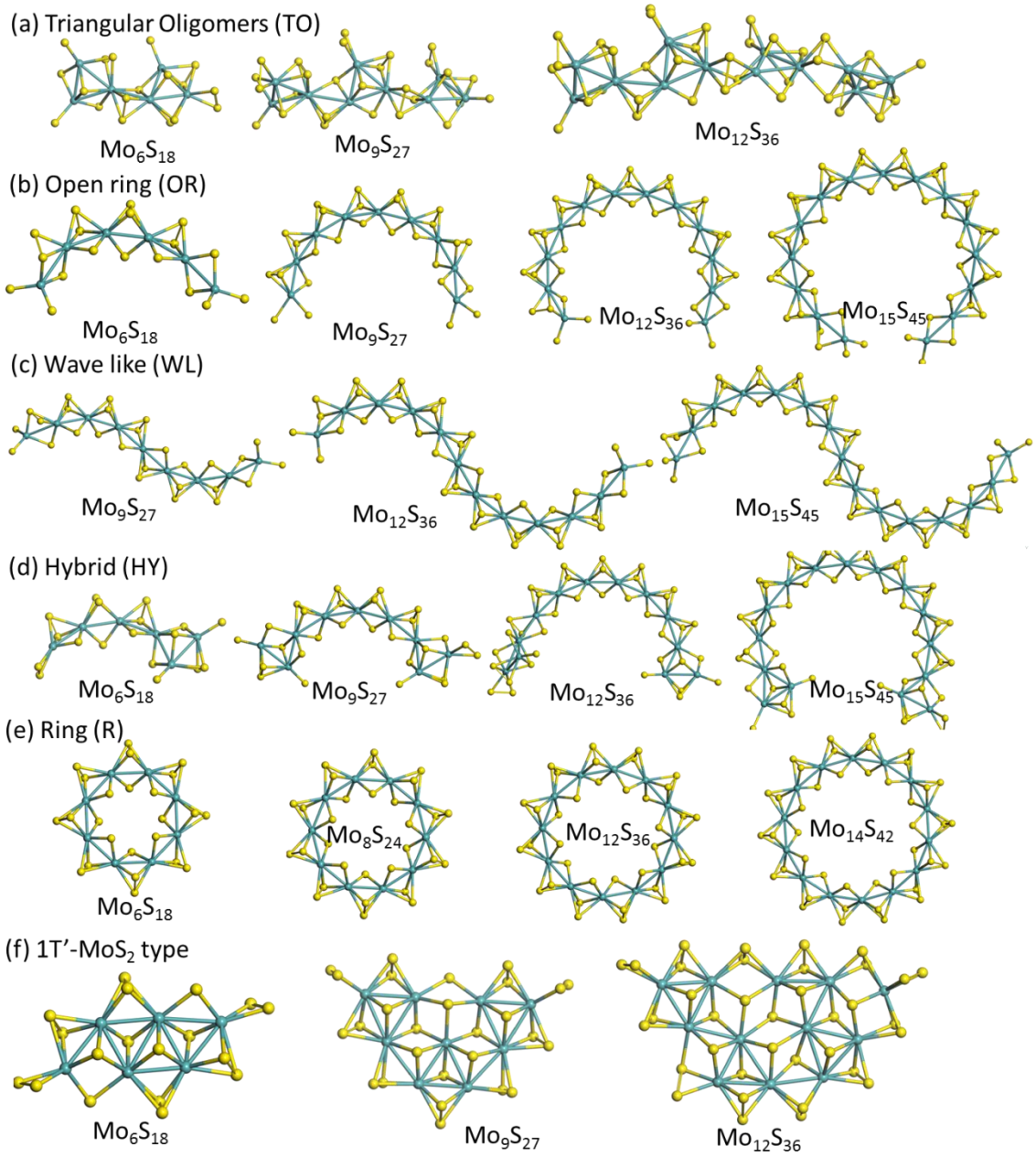

Figure S3:Structural configurations of various different family of 0D-clusters and their stoichiometry.

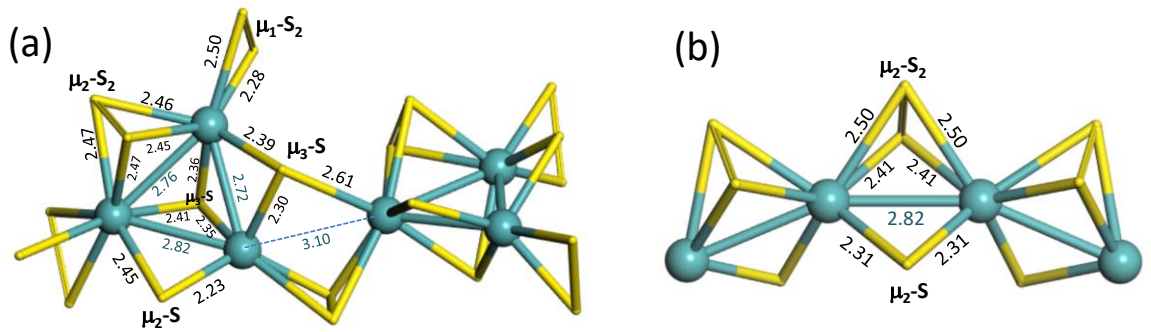

Figure S4: Local structures of (a) 1D-TO-P polymorphs and (b) R-P, 1D-WL-P or 1D-H-P polymorphs. Distances (in Å) represent local values only (not averaged values).

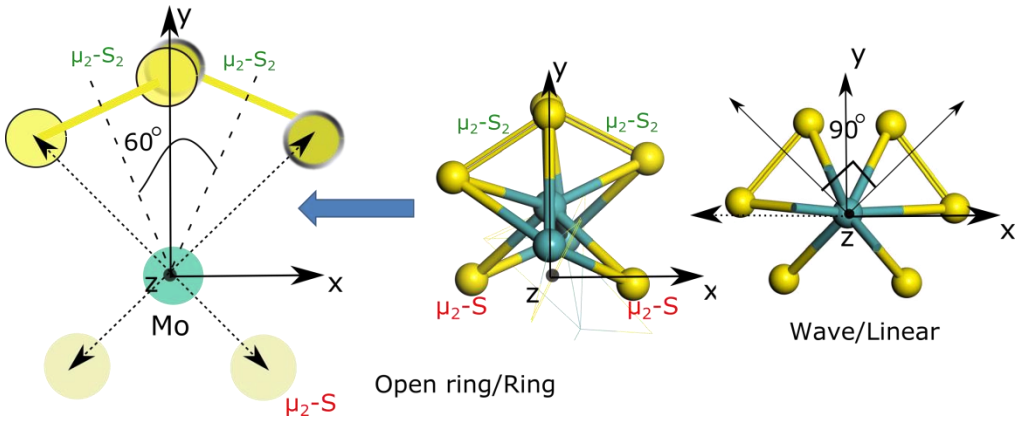

Figure S5: Side view of open-ring (OR) structure and orientation of dimers w.r.t. the plane of Mo-Mo arc (yz plane).

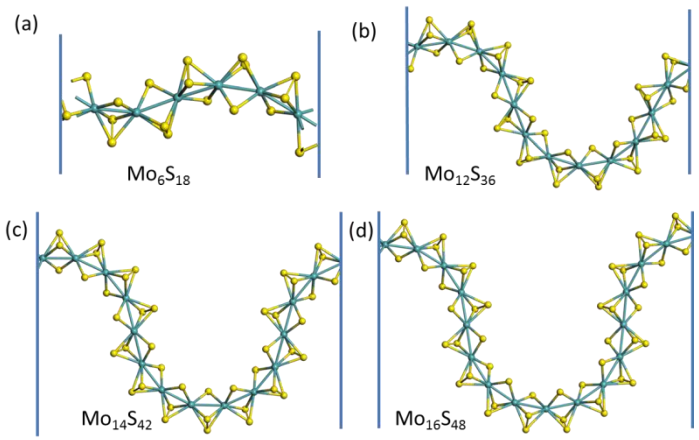

Figure S6: Various 1D-periodic wave like nano-structures with different number of Mo-atoms in unit cell. Corresponding structures with relative energy (w.r.t. per Mo_3S_9 of TO) (a)-2.45, (b) -2.69, (c)-2.71 and (d) -2.72 in eV.

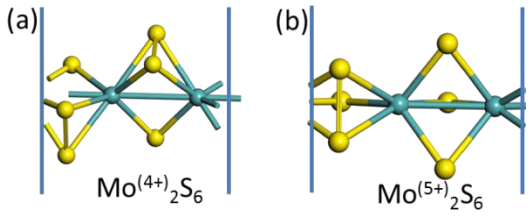

Figure S7: Linear 1D-periodic structures: (a) O.S = +4, R.E. = -1.73 eV, and (b) O.S = +5, R.E. = -1.29 eV. Relative energy is w.r.t. per Mo_3S_9 (TO).

Table S1: Cell parameter for the various periodic structures along the direction of periodicity.

Polymorphs	Cell parameter (Å)
TO-P ($Mo_{18}S_{54}$)	**34.30**
WL-P($Mo_{12}S_{36}$)	**23.86**
WL-P($Mo_{14}S_{36}$)	**24.96**
WL-P($Mo_{16}S_{48}$)	**26.35**
L-P^{4+}(Mo_2S_6)	**5.79**
L-P^{5+}(Mo_2S_6)	**5.98**
NbS_3-ribbon (Mo_4S_{12})	**6.46**

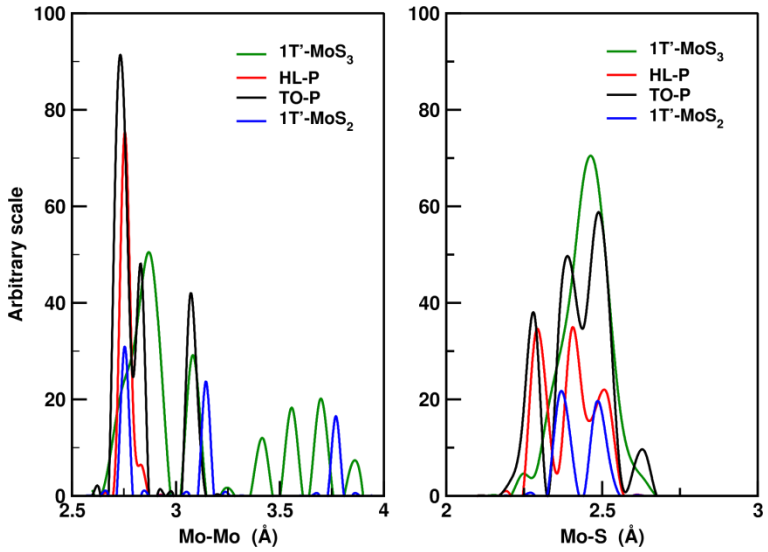

Figure S8: Pair correlation function (PCF) for Mo-Mo and Mo-S bonding distribution for various types of MoS_3 polymorphs.

Note: The Mo-S PCF for TO-P reveals 4 distinct peaks corresponding to the various Mo-S bonds involving the various μ_i-S_j species represented in Figure S4 a. Table 1 reports only two types of Mo-S bonds: one short (2.27 Å) present in μ_2-S and μ_1-S_2 species and one long bond by averaging over μ_2-S, μ_3-S and μ_1-S, μ_2-S_2 (2.44 Å).

For HL-P, the PCF for Mo-S shows that 3 distinct peaks are identified in the HL-P (also true for R and WL structures): one short Mo-S bond (2.31 Å) involving μ_2-S species, and two long bonds fused in one single in Table 1, involving μ_2-S_2 species (Figure S4 b).

Table S2: Average bond lengths of Mo-Mo, Mo-S, S=S for different clusters and in parenthesis number of Mo-Mo bonds presents in the cluster as a function of size.

No of Mo atoms	$Mo\text{-}Mo_{long}$(Å)	$Mo\text{-}Mo_{short}$(Å)	Mo-S (Å)	S-S (Å)
Triangular oligomer (TO)				
3	2.96 (2)	2.72 (1)	2.35	2.05
6	2.95 (2)	2.81 (5)	2.37	2.04
9	3.04 (2)	2.79 (9)	2.36	2.04
12	3.06 (3)	2.78 (12)	2.38	2.04
15	3.10 (4)	2.78 (15)	2.40	2.04
Open Ring (OR)				
3		2.72 (2)	2.39	2.07
6		2.73 (5)	2.40	2.06
9		2.75 (8)	2.40	2.06
12		2.75 (11)	2.40	2.06
15		2.75 (14)	2.41	2.05
Ring (R)				
6		2.79 (6)	2.46	2.05
12		2.73(12)	2.41	2.05
14		2.74(14)	2.41	2.05
16		2.76(16)	2.40	2.05

Table S3: Binding energy (in eV) of different Sulfur species present in various polymorphs by core level shift calculation.

Species	ΔB.E = BE(μ_2-S_2) – BE(μ_1-S_2)	ΔB.E = BE(μ_2-S_2) – BE(μ_1-S)	ΔB.E = BE(μ_2-S_2) – BE(μ_2-S)	ΔB.E = BE(μ_2-S_2) – BE(μ_3-S)
TO	**1.57**	**2.84**	**1.56**	**1.3**
TO-P	**0.75**	--	**0.87**	**1.09**
OR	--	**2.23**	**1.66**	--
WL	--	**2.31**	**1.14**	--
WL-P	--	--	**1.48**	--
HL-P	--	--	**1.75**	--
1T'-MoS_3	**1.55**	--	--	**1.43**

SI.2 AB-INITIO MOLECULAR DYNAMICS

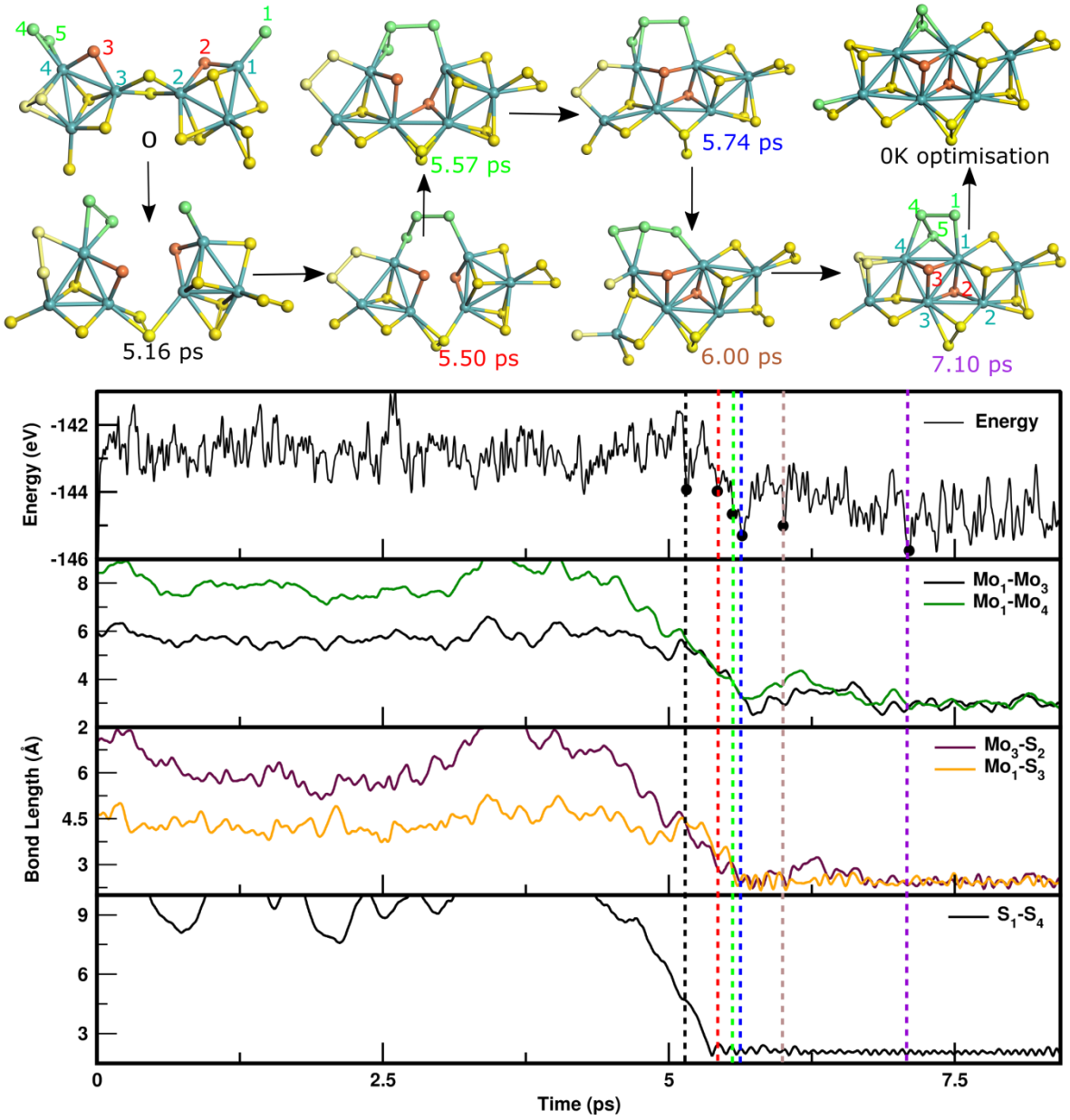

Figure S9: Panel 1: Relevant intermediate structures observed during AIMD simulation (T = 1000 K) of the transformation of Mo_6S_{18} TO into 1T'-MoS_2 like phase. Color legend: Blue balls: Mo atoms, yellow balls: S atoms not directly involved in the transformation, red balls: μ_2-S becoming μ_3-S in the newly formed Mo_3 triangles, green balls: μ_1-S and μ_1-S_2 interacting during MD.

Panel 2: Total energy evolution as a function of time, black dots represent the energy of the intermediate structures given in Panel 1. Panel 3 : Evolution of the Mo-Mo distances for the two newly formed Mo-Mo bonds. Panel 4 : Evolution of the Mo-S distances for the two new formed Mo-S bonds. Panel 5 : Evolution of the S-S distance for the newly formed S_1-S_4 bond distance.

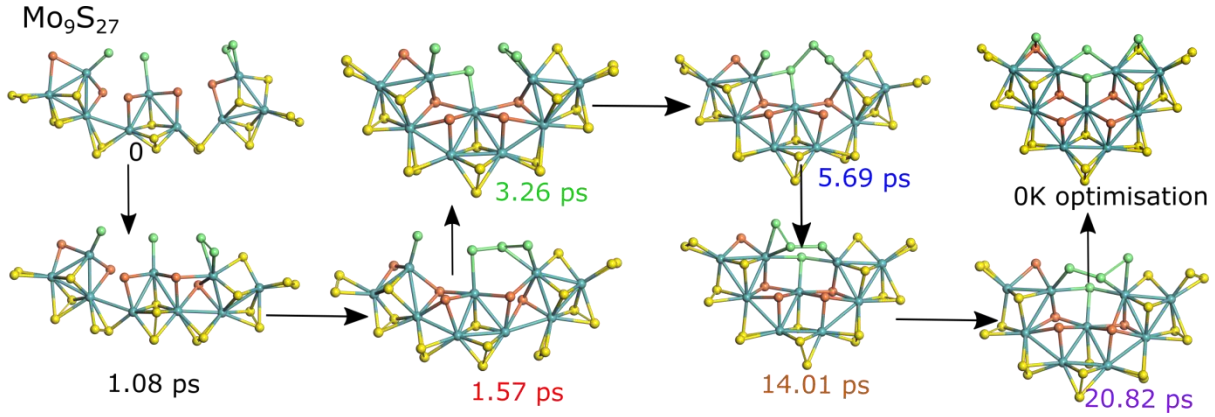

Figure S10: Relevant intermediate structures observed during AIMD simulation (T = 1000 K) of the transformation of Mo_9S_{27} TO into 1T'-MoS_2 like phase. Color legend: Blue balls: Mo atoms, yellow balls: S atoms not directly involved in the transformation, red balls: μ_2-S becoming μ_3-S in the newly formed Mo_3 triangles, green balls: μ_1-S and μ_1-S_2 interacting during MD.

If we now the successive intermediates formed as well as the associated transformation mechanisms revealed in both cases, we notice in Figure S9 and Figure S10, two main families of S species playing a key-role for the formation of the 1T-type MoS_3 structure. The first ones are the μ_2-S atoms (red balls Figure S9 andFigure S10) which are becoming μ_3-S atoms located in the hollow site of the newly formed Mo_3 triangles. As the analysis of the Mo-S distance shows it for the Mo_6S_{18} (see steps 5.50 ps and 5.57 ps and Mo-S distances in Figure S9), the μ_2-S atoms are becoming closer to two Mo-atoms belonging to the two triangular clusters and thus allow the formation of new Mo-S bonds inside the newly formed adjacent triangles. Simultaneously the Mo-Mo distance decreases. It must be also underlined that the relative position of these bridging S-atoms is critical to form the 1T-type pattern since they must become μ_3-S (apical) in the hollow positions located above and below the Mo plane. Otherwise the formation of the 1T-type is impossible.

The other S-atoms involved are μ_1-S and μ_1-S_2 (green balls in Figure S9 andFigure S10) which interact by forming transient S_3 trimers which also help for the condensation mechanisms by bridging the distant triangles close together (steps 5.50 ps and 5.57 ps in Figure S9 and S-S distance).

Finally, it is important to stress that all the μ_2-S_2 remains almost not involved in the transformation. Since they are located at the edges of the cluster, they potentially hinder the growth of the 1T-structure. The present transformation is induced by the thermal effect and it could be accelerated in presence of hydrogen gas which will remove easily some excess S-atoms particularly those of μ_2-S_2 and μ_1-S_2. Such sulfo-reductive conditions are often used to activate the MoS_2 phases experimentally.

Finally, this dynamic evolution of the structure is clearly featured by the energy profile (Figure S9) showing that after 5ps, the energy drops as the oligomer starts to condense and finally reaches a low energy plateau when the 1T-type structure is formed. To compare consistently the energies of these 1T-type structures with the former ones as reported in Figure 3, we perform a static geometry optimization at 0 K on the AIMD structures obtained at the final energy plateau. Figure 3 shows that for three sizes Mo_6S_{18}, Mo_9S_{27} and $Mo_{12}S_{36}$, the 1T-type structures are more stable by -0.56 to -0.73 eV with respect to TO structures.

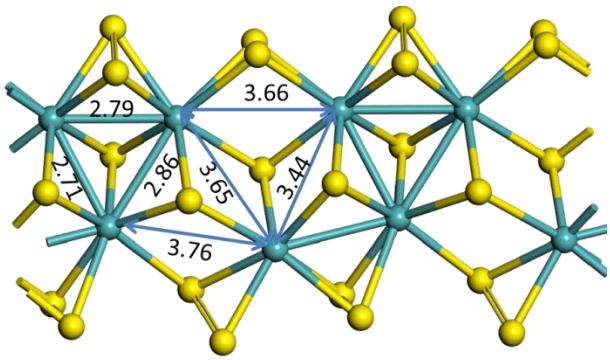

Figure S11: MoS_3 1D-periodic structure (double supercell) inherited from NbS_3 ribbon structure.[2]

SI.3 THERMOCHEMISTRY

To check the effect of thermal and zero point energy corrections; we also incorporate the vibrational entropy contribution and thermal corrections. We assume the rotational and translational degree of freedom will not affect the energetics significantly, so we only take into account the vibrational contribution for the clusters. As we know from classical thermochemistry the free energy can be represented in terms of internal energy of the system and entropy contribution:

$$\Delta G = \Delta U - T\Delta S$$

Where, ΔU includes the sum of electronic energy and zero point energy correction (ZPE). We calculate the ZPE from the sum of all the vibrational modes within the harmonic approximation at 0K.

$$\Delta G = \Delta E_{int} + ZPVE - T\Delta S_{vib}$$

As we are not considering the electronic, rotational, and translational degree of freedom; we only consider the vibrational entropy term and can be computed from following expression:

$$S_{vib} = R\,\Sigma_n \left(\frac{x_n}{e^{x_n}-1} - \ln(1-e^{x_n})\right)$$

Here, $x_n = hc\nu_n/kT$, for the n[th] vibrational mode.[3]

We calculate the corrections for two different temperatures, to check the sensitivity of free energy values with respect to temperature. However, we did not observed any strong effect of these corrections. The effect is very mild for small clusters its negligible and for larger ones, it slightly stabilizes the polymorphs. At 0K, the crossing point between TO and OR occurs after size=9 which is shifted before size=9, for T=625 K. 1T'-MoS_3 polymorphs remains unaffected by thermochemistry.

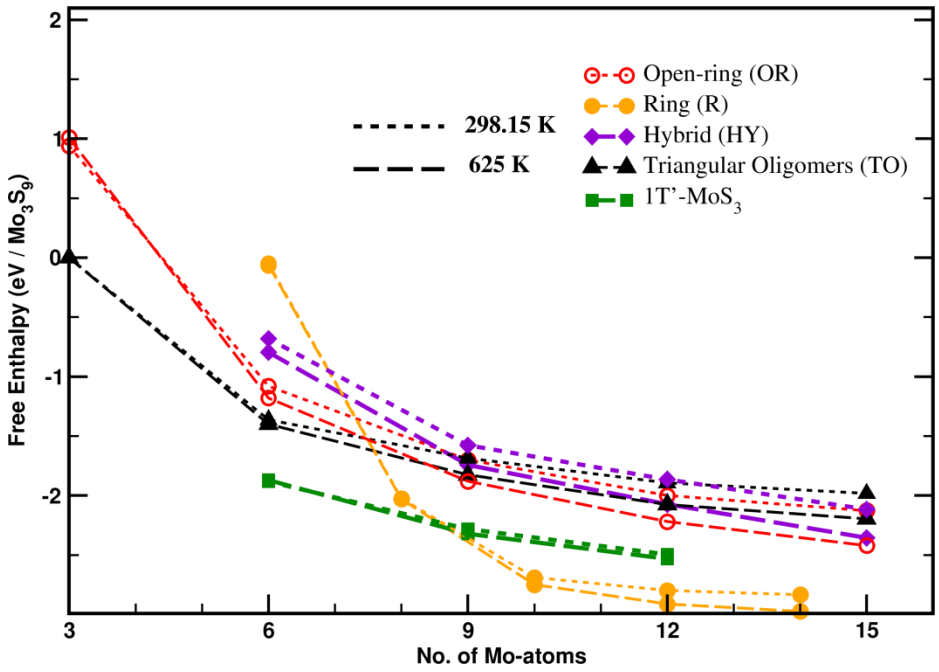

Figure S12: Growth free energy of clusters as a function of number of Mo-atoms including the zero point energy correction and thermal corrections.

SI.4 SPECTROSCOPIC ANALYSIS

SI.4.1 Comparison of the simulation of $[Mo_3S_{13}]^0$, $[Mo_3S_{13}]^{2-}$ and $[Mo_3S_9]^0$ clusters with the reference $[Mo_3S_{13}^{2-}]$ compounds

The current experimental assignment of the characteristic peaks at 470 cm^{-1} refer to μ_3-S (also called apical S), 520 cm^{-1} as μ_1-S_2 (also usually called terminal S_2) and 545 as μ_2-S_2 (bridging S_2) are based on the spectrum of the reference spectrum of $(NH_4^+)_2[Mo_3S_{13}^{2-}].H_2O$.[1] However, as we show in what follows, this interpretation must be considered with great care, due to the fact that firstly, Mo_3S_{13} is fully saturated by S atoms : S/Mo stoichiometry is equal to $4+\frac{1}{3}$ which is far above the one of MoS_3. Secondly, the Mo_3S_{13} entity is negatively charged, whereas *a*-MoS_3 is neutral.[1]

We simulated two species $[Mo_3S_{13}]^0$ and $[Mo_3S_{13}]^{2-}$ to better understand the charge effect on the vibrational frequencies of S-S modes either as μ_1-S_2 or μ_2-S_2 species. The results reported in Table highlight a clear red-shift of the vibrational S-S mode of the μ_1-S_2 species by about 60 cm^{-1} in $[Mo_3S_{13}]^{2-}$ with respect to $[Mo_3S_{13}]^0$. By contrast, the vibrational frequency of μ_1-S_2 mode is not affected by the charge. To delve deeper into this effect, we undertook a Bader charge analysis (Table) revealing that charge accumulates on the terminal μ_1-S_2 species, inducing a S-S bond stretching by 0.029 Å and thus a shift of the vibrational S-S modes to a lower frequency. By contrast, the charge of μ_2-S_2 remains almost constant and thus it results on a weaker change in vibrational frequency. So in the case of the reference $[Mo_3S_{13}]^{2-}$ charged compound, a clear distinction (by about 50 cm^{-1}) can be made between μ_1-S_2 and μ_2-S, whereas this discrimination vanishes for the neutral $[Mo_3S_{13}]^0$. Moreover, effect of the over-stoichiometry is also highlighted in Table since the S-S frequencies in μ_1-S_2 and μ_2-S_2 are also red-shifted by 16/18 cm^{-1} in $[Mo_3S_{13}]^0$ with respect to $[Mo_3S_9]^0$. In addition, two μ_1-S and μ_2-S species are present in $[Mo_3S_9]^0$ with lower frequencies at about 530 and 440-460 cm^{-1} respectively, not present neither in $[Mo_3S_{13}]^0$ nor in $[Mo_3S_{13}]^{2-}$.

Table S4: Bond lengths, Bader charges and vibrational frequency of S_2 and S species present in $[Mo_3S_{13}]^0$, $[Mo_3S_{13}]^{-2}$ and $[Mo_3S_9]^0$

			S-S bond length (Å)	charge on S_2 species	vibrational frequency (cm^{-1})
	Experiment	μ_1-S_2	-	-	505
		μ_2-S_2	-	-	545
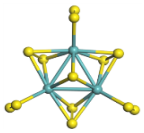	$[Mo_3S_{13}]^0$	μ_1-S_2	1.999	6.29	560
		μ_2-S_2	2.028	6.41	555
		μ_3-S	-	-	436
	$[Mo_3S_{13}]^{2-}$	μ_1-S_2	2.028	6.54	500
		μ_2-S_2	2.032	6.49	550
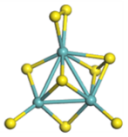		μ_3-S	-	-	431
	$[Mo_3S_9]^0$	μ_1-S_2	2.053	6.64	542
		μ_2-S_2	2.057	6.37	539
		μ_1-S	-	-	532, 527
		μ_2-S	-	-	443, 466
		μ_3-S	-	-	422

As a consequence, the IR assignment of MoS_3 exclusively based on the $(NH_4^+)_2[Mo_3S_{13}^{2-}]$ reference could be seriously misleading. In particular, the usual empirical assignment of the characteristic peaks at 520 cm^{-1} for μ_1-S_2 and 545 cm^{-1} for μ_2-S_2 is not confirmed. From this, we can

thus indicate that the μ_1-S_2 or μ_2-S_2 would be difficult to differentiate, while other species such as μ_1-S or μ_2-S have never been invoked for the IR assignment, whereas they exist in $[Mo_3S_{13}]^0$ as well as in larger TO identified.

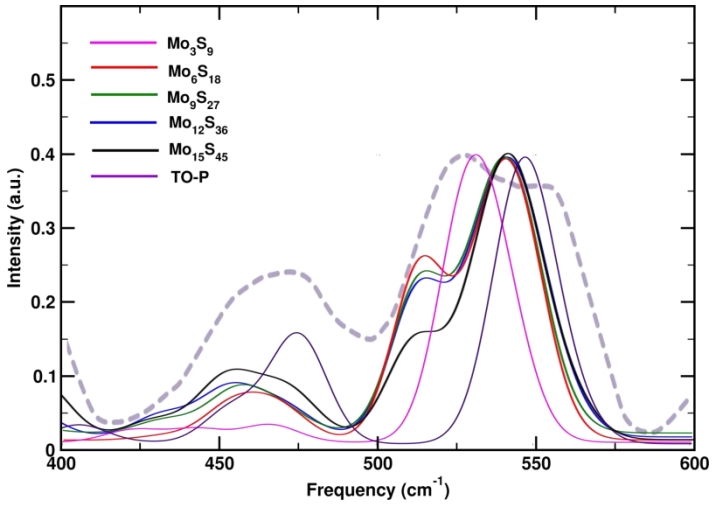

Figure S13: DFPT simulated IR spectrum of various Mo_kS_{3k} TO (solid lines). Experimental IR spectrum (dashed line) from Ref.[1] All simulated spectra have been renormalized while keeping the highest intensity peak fixed.

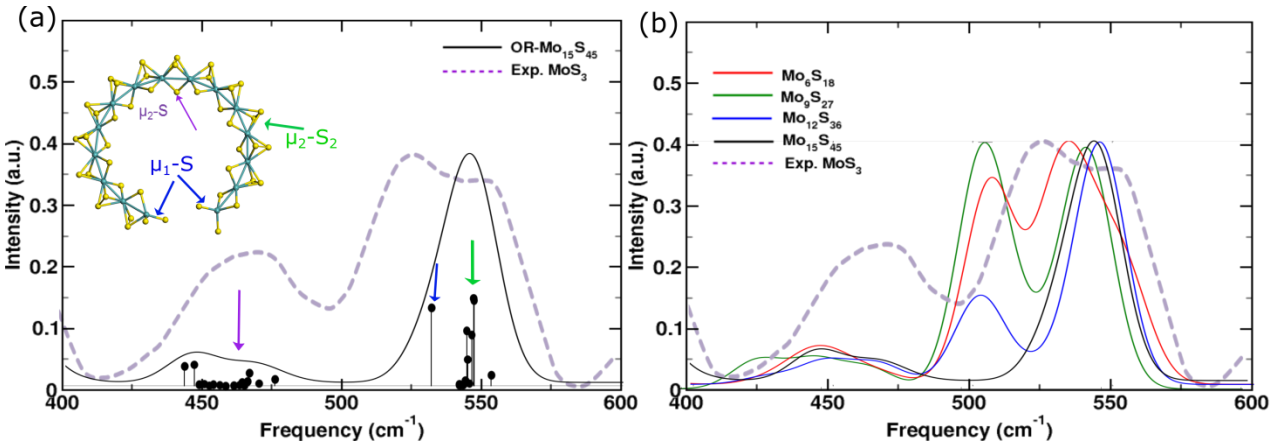

Figure S14: DFPT simulated IR spectrum of open-ring (OR) models (solid lines): a) for $Mo_{15}S_{45}$, b) various Mo_kS_{3k}. All simulated spectra have been renormalized while keeping the highest intensity peak fixed. Experimental IR spectrum (dashed lines) from ref.[1]

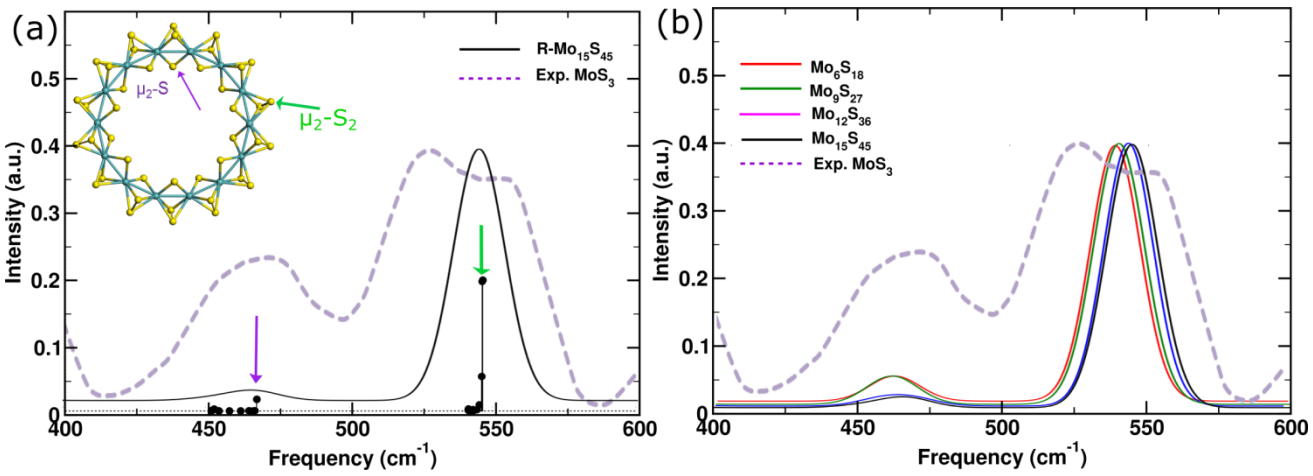

Figure S15: DFPT simulated IR spectrum of ring (R) models (solid lines): a) $Mo_{14}S_{42}$, b) various Mo_kS_{3k}. All simulated spectra have been renormalized while keeping the highest intensity peak fixed. Experimental IR spectrum (dashed lines) from ref.[1]

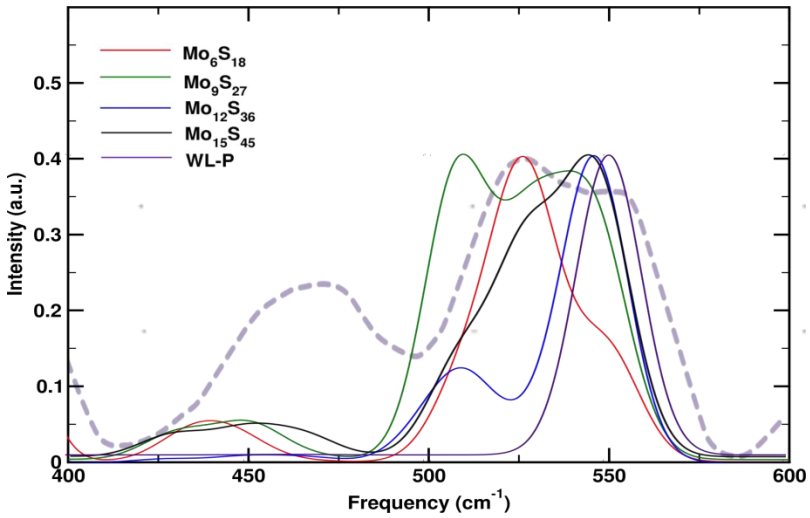

Figure S16: DFPT simulated IR spectrum of various Mo_kS_{3k} Wave-like (WL) polymorphs (solid lines). Experimental IR spectrum (dashed line) from Ref.[1] All simulated spectra have been renormalized while keeping the highest intensity peak fixed.

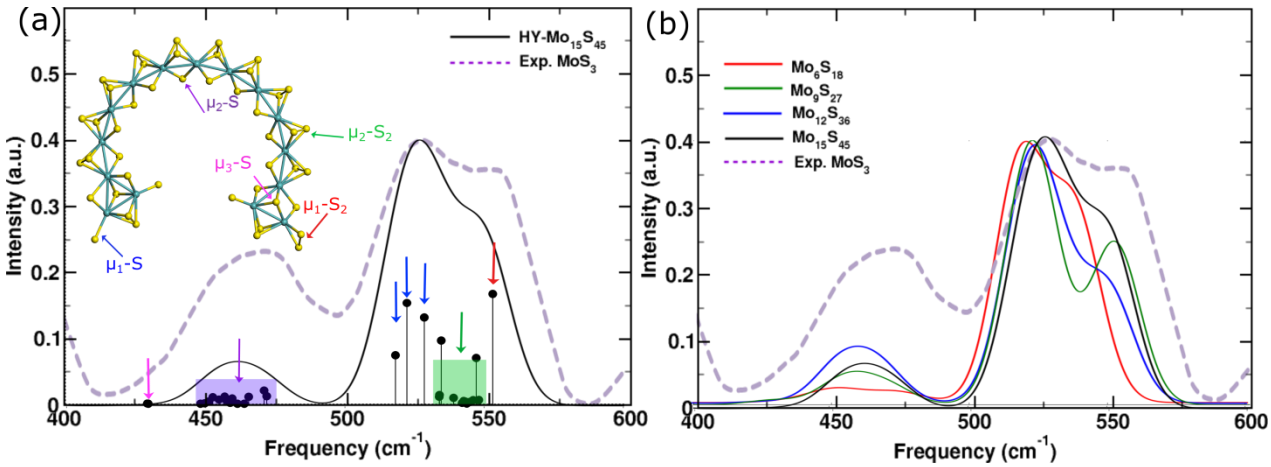

Figure S17: DFPT simulated IR spectrum of hybrid (HY) models (solid lines): a) $Mo_{15}S_{45}$, b) various Mo_kS_{3k}. All simulated spectra have been renormalized while keeping the highest intensity peak fixed. Experimental IR spectrum (dashed lines) from ref.[1]

Table S5: Calculated vibrational frequencies of the various μ_x-S_y species present in the different oligomeric models as a function of size.

No of Mo atoms	μ_2-S_2(cm^{-1})		μ_1-S_2 (cm^{-1})	μ_1-S (cm^{-1})	μ_2-S(cm^{-1})	μ_3-S(cm^{-1})
Triangular oligomer (TO)						
	μ_2-S_2 bridging two triangles	μ_2-S_2 in triangles				
3		539	542	527, 532	443, 466	422
6	539	549-555	573	507, 526,533	447-464	421, 429
9	535-537	545-557	539-544	512, 533	455-471	427-432
12	535-538	547-558	538-546	512, 533	447-453	426-432
15	537-538	555-558	538-545	512, 533	446-475	425-432
Open ring (OR)						
6	541-555			531, 507, 504	470-451	
9	541-547			523, 507, 502	443-469	
12	542-548			526, 509	443-468	
15	541-553			531, 508, 502	443-475	

No of Mo atoms	μ_2-S_2(cm^{-1})		μ_1-S_2 (cm^{-1})	μ_1-S (cm^{-1})	μ_2-S(cm^{-1})	μ_3-S(cm^{-1})
Hybrid (HY)						
	μ_2-S_2 in chain	μ_2-S_2 in triangles				
6	533-545	535	539-549	517,521	449 - 479	433
9	532-547	533,538	553	517,522,527	450 - 472	428,429
12	533-548	533,538	553	518,522,528	449 - 470	428,431
15	533-547	534,538	552	517,522,527	447 - 472	429,429
Ring (R)						
6	537-542				465-467	
12	541-544				454-467	
14	540-546				451-467	
16	541-547				449-466	
Wave Like (WL)						
15	542-553			527, 511, 508	467-435	
1T'-MoS_3						
12	534-554		558,561	503		416-468